Journal of Cerebral Blood Flow & Metabolism (2010) 30, 370–380

www.jcbfm.com

Cyclooxygenase-1 and -2 differentially modulate lipopolysaccharide-induced blood–brain barrier disruption through matrix metalloproteinase activity

Saba Aid[1,4], Afonso C Silva[2,4], Eduardo Candelario-Jalil[3], Sang-Ho Choi[1], Gary A Rosenberg[3] and Francesca Bosetti[1]

[1]*Brain Physiology and Metabolism Section, National Institute on Aging, NIH, Bethesda, Maryland, USA;* [2]*Cerebral Microcirculation Unit, National Institute of Neurological Disorders and Stroke, NIH, Bethesda, Maryland, USA;* [3]*Department of Neurology, University of New Mexico, Health Sciences Center MSC10 5620, Albuquerque, New Mexico, USA*

Cyclooxygenases (COX) -1 and -2 are key regulators of innate immune responses. We recently demonstrated that the expression of proinflammatory cytokines and chemokines is reduced in COX-1 null ($^{-/-}$), and increased in COX-2$^{-/-}$ mice compared with their respective wild type controls during lipopolysaccharide (LPS)-induced innate immune activation. As chemokines are involved in leukocyte recruitment into the inflamed brain, we hypothesized that COX-1 and COX-2 deletion will differentially modulate blood–brain barrier (BBB) permeability in response to LPS. In the present study, using quantitative magnetic resonance imaging, we found that LPS-induced BBB disruption was exacerbated in COX-2$^{-/-}$ versus COX-2$^{+/+}$ mice. In the hippocampus and cortex of LPS-treated mice, matrix metalloproteinase (MMP)-3 activity was significantly decreased in COX-1$^{-/-}$ mice, whereas in COX-2$^{-/-}$ mice the activity of both MMP-9 and MMP-3, known to mediate BBB breakdown, was increased. Brain mRNA expression of the leukocyte attracting chemokine Cxcl10, the intercellular interaction molecule Icam-1, the pan-leukocyte marker Cd45 was increased in COX-2$^{-/-}$ versus COX-2$^{+/+}$ mice, whereas Cxcl10 and Cd45 mRNA expression was decreased in COX-1$^{-/-}$ versus COX-1$^{+/+}$ mice after LPS. Altogether, these results indicate that COX-2 activity modulates MMP-9 and-3 activities and is necessary to maintain BBB integrity during toll-like receptor 4-dependent innate immune activation.
Journal of Cerebral Blood Flow & Metabolism (2010) **30,** 370–380; doi:10.1038/jcbfm.2009.223; published online 21 October 2009

Keywords: blood–brain barrier; cyclooxygenases; lipopolysaccharide; matrix metalloproteinases; MRI; neuroinflammation

Introduction

The blood–brain barrier (BBB) is a structural and functional barrier that is formed by the tight apposition of the brain microvascular endothelium, connected by intercellular tight junctions, which limits the entry of plasma components, red blood cells, and leukocytes into the brain (Zlokovic, 2008). This highly specialized endothelium and the surrounding cells (pericytes, astrocytes, and microglia) constitute the neurovascular unit. Disruption of the BBB integrity occurs during inflammatory conditions of the central nervous system, as observed in multiple sclerosis, bacterial meningitis, stroke, and Parkinson's disease (Weiss *et al*, 2009). Alteration of the vascular endothelial permeability is thought to result from the release of cytokines, free radicals, matrix metalloproteinases (MMPs), nitric oxide, and products of arachidonic acid metabolism (Rosenberg, 2002). MMPs have been shown to mediate BBB disruption and to contribute to the neuroinflammatory response by interacting with cytokines (Candelario-Jalil *et al*, 2009; Rosenberg, 2002).

Neuroinflammation, which involves production of cytokines, chemokines, and reactive oxygen species, can be modeled *in vivo* by intracerebroventricular

Correspondence: Dr F Bosetti, Brain Physiology and Metabolism Section, National Institute on Aging, National Institutes of Health, 9 Memorial Drive, Room 1S126 MSC 0947, Bethesda, MD 20892, USA.
E-mail: frances@mail.nih.gov
[4]These authors contributed equally to this work.
Received 23 June 2009; revised 28 August 2009; accepted 23 September 2009; published online 21 October 2009

injection of lipopolysaccharide (LPS) (Aid *et al*, 2008; Choi *et al*, 2008; Keene *et al*, 2009; Rosenberg, 2002). Pathophysiological events occurring in this experimental model include activation of MMP-9 (gelatinase B) and MMP-3 (stromelysin-1), and BBB breakdown (Gurney *et al*, 2006; Mun-Bryce and Rosenberg, 1998).

Prostaglandin endoperoxide synthases or cyclooxygenases (COX-1 and COX-2) are the pharmacological targets of nonsteroidal antiinflammatory drugs (NSAIDs), commonly used to treat pain and inflammation. COXs have a central role in the inflammatory cascade by converting arachidonic acid, released from membrane phospholipids by a phospholipase A_2, into bioactive prostanoids. Data on the role of each COX isoform in BBB permeability are limited and sometimes conflicting. For example, post treatment with COX inhibitors showed contrasting roles of the COX isoforms on BBB disruption in models of neuroinflammation and ischemic stroke, depending on the selectivity of the NSAIDs and the model used (Candelario-Jalil *et al*, 2007*a*, *b*). The use of pharmacological inhibitors is complex, as one needs to consider the different ability of various NSAIDs to inhibit one COX isoform versus the other, possible off-target effects, as well as the route of administration, dosage, and duration of treatment. To this end, the use of knockout mice is advantageous in allowing full characterization of the specific roles of each COX isoform on BBB breakdown in response to LPS-induced neuroinflammation.

We demonstrated earlier that brain expressions of cytokines and chemokines were decreased in COX-1-deficient (COX-$1^{-/-}$) mice and increased in COX-2-deficient (COX-$2^{-/-}$) compared with their respective wild-type mice during LPS-induced innate immune activation (Aid *et al*, 2008; Choi *et al*, 2008). As chemokines are involved in the trafficking and the recruitment of leukocytes into the inflamed brain, and cytokines contribute to alter the neurovascular unit, we hypothesized that COX-1 and COX-2 will have distinct roles on the modulation of LPS-induced BBB disruption. To test this hypothesis, we used gadolinium-enhanced magnetic resonance imaging (MRI) to quantify LPS-induced BBB damage in the brain of COX-1- or COX-2-deficient mice. We also showed that LPS-induced BBB damage, as well as vascular and glial indicators of BBB integrity, correlated with MMP-9 and MMP-3 activities.

Materials and methods

Animals Housing

Four to six-month-old male COX-$1^{+/+}$, COX-$1^{-/-}$, COX-$2^{+/+}$, and COX-$2^{-/-}$ mice on a C57BL/6-129/Ola genetic background were used. Mice were received at our animal facility at 10 weeks of age from an NIEHS (National Institute of Environmental Health Sciences) colony maintained by Taconic Farms (Germantown, NY, USA) with heterozygous by heterozygous breedings for greater than 35 generations. To prevent the inclusion of strain or genetic background confounders between COX null and wild-type mice, all of the mice used in this study were progeny derived from heterozygous by heterozygous mating and therefore all contained the same strain and genetic background (Toscano *et al*, 2007). Mice were housed at 25°C in our animal facility with a 12 h light/dark cycle with free access to food and water. All procedures were performed under the NIH-approved animal protocols in accordance with the NIH guidelines on the care and use of laboratory animals.

Stereotaxic Surgery and Intracerebroventricular Injection of LPS

Mice were anesthetized with ketamine (100 mg/kg) and xylazine (10 mg/kg, i.p.) and positioned in a stereotaxic apparatus (Kopf Instruments, Tujunga, CA, USA). Vehicle (sterile phosphate buffer saline, 5 μL) or LPS (LPS was TCA extracted from *Escherichia coli* serotype 055:B5 (Sigma-Aldrich, St Louis, MO, USA); 5 μg in 5 μL of vehicle) was administered into the cerebral lateral ventricle using a 10 μL syringe with a 33 gauge needle (World Precision Instruments, Sarasota, FL, USA) and a syringe pump (Stoelting, Wood Dale, IL, USA) at a rate of 1 μL/mins. This dose of LPS has been shown by us and by others to produce significant neuroinflammation 24 h after injection (Aid *et al*, 2008; Choi *et al*, 2008; Goralski *et al*, 2005; Milatovic *et al*, 2004). The coordinates for the stereotaxic injections were −2.3 mm dorsal/ventral, −1.0 mm lateral, and −0.5 mm anterior/posterior from the bregma (Paxinos and Franklin, 2001). The needle was kept in this position for an additional 5 mins after injection and then retrieved slowly from the brain.

Magnetic Resonance Imaging

Twenty-four hours after intracerebroventricular injection of LPS, mice were anesthetized by breathing freely oxygen-enriched air ($FiO_2 \sim 50\%$) containing isoflurane (5% induction followed by 1.5% to 2% maintenance. Rectal temperature was monitored and maintained at 37.5 ± 0.5°C by means of a feedback-regulated MRI-compatible electric bed (Rapid Biomedical GmbH, Rimpar, Germany). Real-time monitoring of physiologic parameters (rectal temperature, pulse oximetry, end-tidal CO_2, heart rate, and respiratory rate) was performed during the entire duration of the study. A PE-10 catheter was placed into the lateral tail vein of each animal for injection of the contrast agent gadolinium-diethylenetriaminepentaacetic acid (Gd-DTPA). MRI with Gd-DTPA has been used both in rodents (Candelario-Jalil *et al*, 2007*b*) and in humans to assess BBB disruption associated with stroke, brain injury, and multiple sclerosis (Mikulis and Roberts, 2007; Takanashi *et al*, 2000).

MRI was performed on a 7 T/30 cm USR Bruker AVI MR scanner (Bruker Biospin, Billerica, MA, USA), equipped with a 150 mm ID gradient set capable of 450 mT/m and slew rates of 3,000 T/(m secs) (Resonance Research Inc., Billerica, MA, USA). A transmit-only linear radio-frequency coil (i.d., 120 mm) was used for magnetic resonance (MR) excitation, and a dedicated 10 mm i.d. elliptical surface radio-frequency coil was used for signal acquisition. Initial localizer images were acquired using the following parameters: 2D RARE; TR/TE_{eff}, 12,000/67 ms; matrix, 256×256 (RARE factor 16); field of view (FOV), 2.56 cm; slice thickness, 0.5 mm; and one slice per orientation. After the localizer images were acquired, localized shimming over the entire brain was performed using the FASTMAP sequence (Gruetter, 1993), and a new set of T_2-weighted imaging was performed with the same parameters listed above over 24 consecutive coronal slices to serve as an additional reference scan and to identify the slice containing the LPS injection site. Once the LPS injection site was identified, 16 consecutive 0.5 mm-thick slices, running from approximately 4 mm anterior to 4 mm posterior to Bregma, were chosen for further data acquisition. High resolution spin-echo, T_1-weighted MRI were acquired using the following parameters: TR/TE, 250/8.67 ms; matrix, 256×256; FOV, 2.56 cm; slice thickness, 0.5 mm; 16 slices; nominal spatial resolution, $100 \times 100 \times 500\,\mu m^3$; total acquisition time 2 mins 8 secs. Interleaved with the T_1-weighted images, we also acquired quantitative T_1 maps from the 8 innermost slices within the 16-slice set, using the following parameters: pulse sequence, spin-echo echo-planar imaging; preparation, inversion recovery; TR/TE, 10,000/27 ms; matrix, 64×64; FOV, 2.56 cm; slice thickness, 0.5 mm; 8 slices; nominal spatial resolution, $400 \times 400 \times 500\,\mu m^3$; total acquisition time 6 mins 40 secs. For the T_1 mapping, 20 inversion times (TI) were used, according to $TI\ (n) = (50 + 500 \times n)$ ms, where $n = 0, 1, 2, 19$. The MR protocol for evaluating BBB permeability consisted of a reference baseline acquisition using both the T_1-weighted MRI and the fast T_1 mapping echo-planar imaging sequence. Mice were then injected with 2.0 mmol/kg Gd-DTPA (molecular mass = 938 Da; Berlex, Montville, NJ, USA) as a 0.1 mL bolus into the lateral tail vein through an indwelling catheter, followed by imaging with both the T_1-weighted MRI and the fast T_1 mapping echo-planar imaging sequences, collecting 16 in an interleaved manner over 45 mins.

The acquired MRI data were transferred to a dedicated computer workstation for post processing. Post processing of the raw data involved generating T_1 maps from the raw data, reconstruction of permeability coefficient maps, and construction of the Patlak plots according to the methodology described in Patlak *et al* (1983). All the data processing was performed using in-house software written in MATLAB (Mathworks, Natick, MA, USA). Image analysis was performed using ImageJ (NIH, Bethesda, MD, USA) and Stimulate software. Region of interest analysis was performed by manually assisted segmentation of the hippocampus using routines written in MATLAB.

RNA Extraction and Quantitative Real-Time PCR

Total RNA was extracted from the whole brain using RNeasy Lipid Tissue Midi kit (Qiagen, Valencia, CA, USA). Briefly, 5 μg of total RNA were reverse transcribed using a High Capacity cDNA Archive kit (Applied Biosystems, Foster City, CA, USA). Quantitative PCR for tissue inhibitor of metalloproteinase-1 (Timp-1), intercellular adhesion molecule-1 (Icam-1), chemokine (C-X-C motif) ligand 10 (Cxcl10), and lymphocyte common antigen (ptprc or Cd45) was performed using specific FAM™ dye-labeled TaqMan gene expression assays (Applied Biosystems) with an ABI PRISM 7000 Sequence Detection System (Applied Biosystems). Data were analyzed using the comparative threshold cycle ($\Delta\Delta Ct$) method (Livak and Schmittgen, 2001), and results were normalized with phosphoglycerate kinase 1 (Pgk1) as an endogenous control and expressed as fold difference from the vehicle-injected respective wild-type mice, as reported earlier (Aid and Bosetti, 2007; Aid *et al*, 2008; Choi *et al*, 2008).

Gelatin-Substrate Zymography

For zymography, tissues were homogenized in a lysis buffer containing 50 mmol/L Tris-HCl pH 7.6, 150 mmol/L NaCl, 5 mmol/L $CaCl_2$, 0.05% Brij-35, 1% Triton X-100, and 0.02% NaN_3. Protein concentration in the homogenate was determined using the Micro BCA Protein Assay kit (Pierce, Rockford, IL, USA). MMP-2 and MMP-9 in the homogenate were concentrated with Gelatin-Sepharose 4B beads (GE Healthcare Biosciences, Piscataway, NJ, USA), and analyzed by gelatin zymography as described earlier (Candelario-Jalil *et al*, 2007*b*). Briefly, 800 μg of total protein in 500 μL was incubated with 80 μL of Gelatin-Sepharose 4B beads for 1 h at 4°C with gentle agitation. The beads were collected and the gelatinases were eluted by incubating with 80 μL of elution buffer (10% DMSO in phosphate-buffered saline) for 30 mins at 4°C with gentle shaking. Equal amount of samples (20 μL) were mixed in a loading buffer containing 80 mmol/L Tris-HCl pH 6.8, 4% sodium dodecyl sulfate, 10% glycerol, and 0.01% bromophenol blue. Samples were electrophoretically separated on 10% sodium dodecyl sulfate-polyacrylamide gels copolymerized with 1 mg/mL gelatin (Sigma-Aldrich, St Louis, MO, USA) under nonreducing conditions. Gels were washed in 2.5% Triton X-100 and then incubated for 40 h at 37°C in a developing buffer containing 50 mmol/L Tris pH 7.6, 5 mmol/L $CaCl_2$, 0.2 mmol/L NaCl, and 0.02% Brij-35. After incubation, gels were stained with 0.125% Coomassie Brilliant Blue R-250 (Sigma-Aldrich) for 30 mins in 10% acetic acid and 50%

methanol. Gels were destained with a solution containing 10% acetic acid and 10% methanol until clear bands of gelatinolysis appeared on a dark blue background. To confirm that detected activities were zinc-dependent gelatinases, some zymogram gels were incubated with developing solution in the presence of 10 mmol/L EDTA. Disappearance of lytic bands in these gels confirmed the metal dependence of gelatinolytic activity characteristic of MMPs. The gels were dried and densitometrically scanned (Alpha Imager 2200; Alpha Innotech, San Leandro, CA, USA). Molecular weights were determined by both protein standards (Bio-Rad Laboratories, Hercules, CA, USA), and conditioned media from HT1080 human fibrosarcoma cells, a well-known source of MMP-2 and -9. In addition, a mixture of active MMP-2 and -9 standards (Chemicon International, Temecula, CA, USA) were used as gelatinase controls. Data were expressed as relative lysis units.

Fluorometric Assay of MMP-3 Enzymatic Activity

The activity of MMP-3 (stromelysin-1) was measured fluorometrically using a 5-carboxyfluorescein (5-FAM)/QXL520 fluorescence resonance energy transfer peptide (AnaSpec Inc., San Jose, CA, USA). In the intact fluorescence resonance energy transfer peptide [5-FAM-Arg-Pro-Lys-Pro-Val-Glu-Nva-Trp-Arg-Lys(QXL520)-NH_2], the fluorescence of 5-FAM is quenched by QXL520. On cleavage into two separate fragments by the MMP-3 present in the sample, the fluorescence of 5-FAM is recovered and can be monitored at excitation/emission wavelengths of 490/520 nm. This peptide has been documented to be cleaved by only MMP-3 and MMP-12 (macrophage elastase) but not by other MMPs (Nagase *et al*, 1994). Brain homogenates containing 100 μg of protein (aliquot from the lysate prepared for zymography) were mixed with assay buffer (50 mmol/L Tris-HCl, pH 7.6, 200 mmol/L NaCl, 5 mmol/L $CaCl_2$, 20 μmol/L $ZnSO_4$, and 0.05% Brij-35) containing the fluorescence resonance energy transfer peptide (1 μmol/L final concentration) to a final volume of 200 μL. The change in fluorescence (expressed as relative fluorescence units) was monitored at 5-mins intervals for 1 h at 37°C using a luminescence spectrometer (model LS55; PerkinElmer Instruments, Buckinghamshire, UK) attached to a workstation running FL WinLab software. For each sample, a linear regression was calculated using Sigma Plot for Windows, version 11.0 (Systat software, Inc., San Jose, CA, USA) and the mean velocity was calculated for each group.

Statistics

Data were expressed as mean ± s.e.m. Raw data obtained from MRI and MMP-9 activity were analyzed using Student's *t*-test. MMP-3 activity was analyzed using two-way ANOVA followed by a posttest Bonferroni when $P<0.05$. For gene expression, log-transformed $2^{-\Delta\Delta Ct}$ values were analyzed using two-way ANOVA (followed by a posttest Bonferroni). *P*-values <0.05 were considered statistically significant. Statistical analysis was performed using the program GraphPad Prism for Windows, version 4.0 (GraphPad Software Incorporated, San Diego, CA, USA).

Results

LPS-Induced BBB Disruption Is Exacerbated in COX-$2^{-/-}$ Mice

Using a quantitative MRI technique, we found that intracerebroventricular LPS induced an increased BBB permeability to Gd-DPTA at 24 h, which is in agreement with previous data obtained by others using biochemical techniques (Gurney *et al*, 2006; Mun-Bryce and Rosenberg, 1998). Figure 1A shows color-coded permeability coefficient (K_i) maps, expressed in mL/100g/min, for four representative mice. The top row shows the K_i maps for two LPS-injected COX-$2^{+/+}$ mice, whereas the bottom row shows K_i maps for two LPS-injected COX-$2^{-/-}$ mice. Four consecutive 1 mm-thick coronal brain sections are shown from each mouse to follow the spatial extent of the gadolinium leakage into the brain. LPS injection into the right cerebral lateral ventricle causes a significant increase in BBB permeability to gadolinium compared with injection of vehicle (data not shown). Even though the increase in BBB permeability favors the right hemisphere of the brain, it spreads both posterior and anterior from the injection site. Therefore, whole brain analysis was performed to assess the effects of LPS on BBB breakdown in the different mice genotypes. The mean K_i was significantly higher in the whole brain of LPS-injected COX-$2^{-/-}$ mice compared with COX-$2^{+/+}$ mice (Figure 1B). Previously, we have shown that LPS causes neuronal damage and glial activation in the hippocampus (Aid *et al*, 2008; Choi *et al*, 2008). Therefore, we performed region-of-interest analysis to assess the effects of LPS on BBB disruption in the hippocampus. We found that the mean K_i was also higher in the hippocampus of COX-$2^{-/-}$ mice compared with COX-$2^{+/+}$ mice after treatment with LPS (Figure 1B). Figure 1C shows the K_i maps for two LPS-injected COX-$1^{+/+}$ mice, whereas the bottom row shows K_i maps for two LPS-injected COX-$1^{-/-}$ mice. Although the mean K_i was not significantly different in the whole brain of LPS-injected COX-$1^{-/-}$ mice compared with COX-$1^{+/+}$ mice (Figure 1D), there was a trend to a decrease ($P=0.06$) in the hippocampus of COX-$1^{-/-}$ 24 h after intracerebroventricular LPS (Figure 1D).

MMP-9 Gelatinolytic Activity Is Increased in COX-$2^{-/-}$ Mice 24 h After LPS

As gelatinase B (MMP-9) is involved in BBB disruption during LPS-induced neuroinflammation (Mun-Bryce and Rosenberg, 1998), we investigated

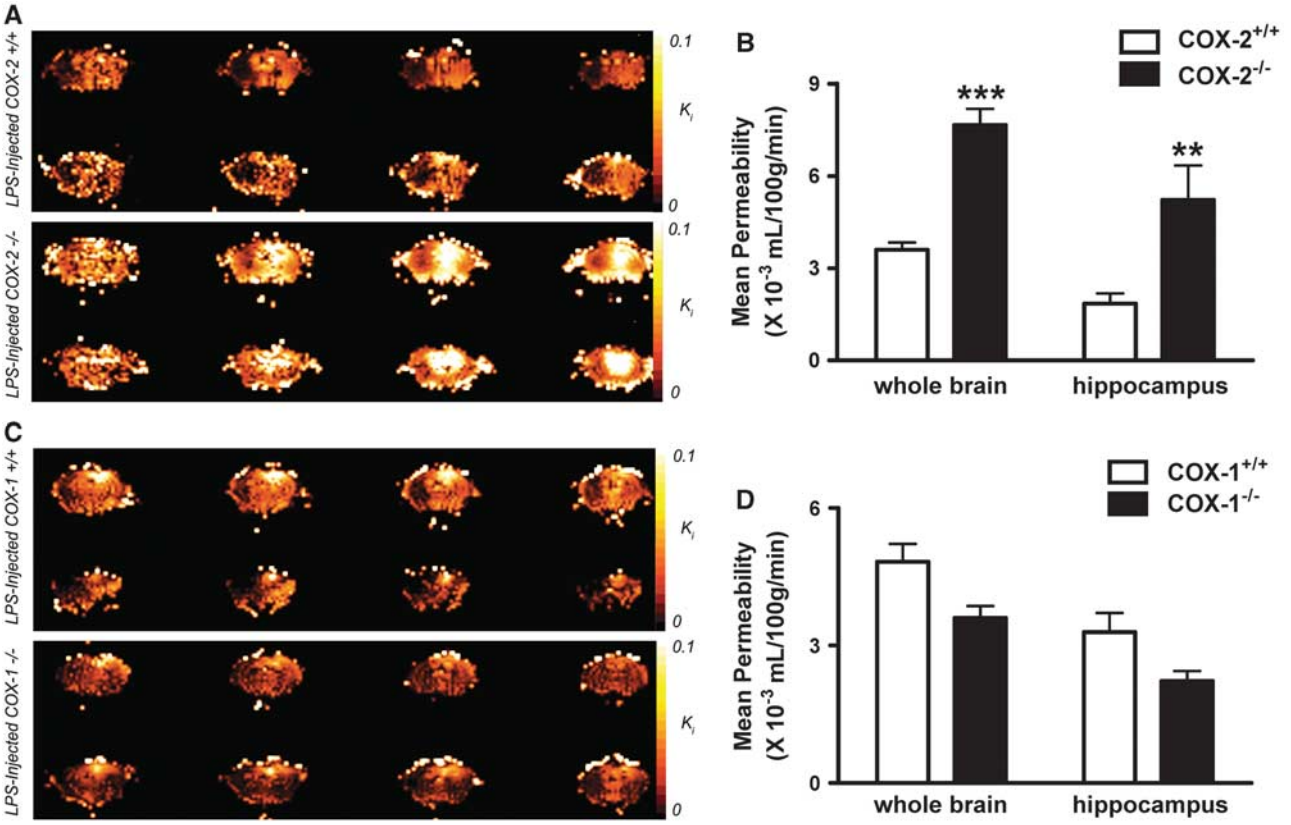

Figure 1 Effects of COX-2 and COX-1 deficiency on LPS-induced increase in BBB permeability, using gadolinium-enhanced magnetic resonance imaging. (**A**) Representative color-coded permeability coefficient map: LPS-injected COX-$2^{+/+}$ mice (top two rows) and LPS-injected COX-$2^{-/-}$ mice (bottom two rows). Four consecutive 1 mm-thick coronal brain sections are shown for each mouse. (**B**) Plot of mean permeability coefficient estimates K_i (mL/100g/min) in the whole brain and in the hippocampus obtained by Patlak Plot analysis in LPS-injected COX-$2^{+/+}$ (white bars) and LPS-injected COX-$2^{-/-}$ mice (black bars). (**C**) Representative color-coded permeability coefficient map: LPS-injected COX-$1^{+/+}$ mice (top two rows) and LPS-injected COX-$1^{-/-}$ mice (bottom two rows). (**D**) Plot of mean permeability coefficient estimates K_i (mL/100g/min) in the whole brain and in the hippocampus obtained by Patlak Plot analysis in LPS-injected COX-$1^{+/+}$ (white bars) and LPS-injected COX-$1^{-/-}$ mice (black bars). Data are presented as mean ± s.e.m. ($n = 5$ to 6). $^{***}P < 0.001$, $^{**}P < 0.01$ versus LPS-injected respective wild-type mice.

the effects of COX-1 or COX-2 deletion on MMP-9 activity in hippocampus and cerebral cortex, 24 h after intracerebroventricular injection of LPS. We used gelatin zymogram to assess the activity of MMP-9 as measured by the densitometric analysis of the 98 kDa band. Previous studies reported that only the full-length form of MMP-9 is detected in biologic samples (active enzyme containing a propeptide domain) (Candelario-Jalil *et al*, 2007*b*; Fridman *et al*, 2003).

No MMP-9 band was detected in hippocampus or cerebral cortex of naïve COX-1- and COX-2- deficient and wild-type mice, even after 48 h incubation of the gels (Figure 2A); however, a band around 72 kDa corresponding at the constitutive MMP-2 was detected in both brain areas and genotype (Figure 2A). Intracerebroventricular injection of LPS produced a significant increase in MMP-9 activity after 24 h compared with the vehicle-injected control, as revealed by gelatin zymography (Figure 2B). Deletion of COX-2 produced a significant increase in the gelatinolytic activity of MMP-9, both in hippocampus and cerebral cortex (Figures 2C and 2D). In contrast, COX-1 deletion did not affect significantly the gelatinolytic activity of MMP-9 in the hippocampus (Figure 2E, $P = 0.09$) or in the cerebral cortex (Figure 2F; $P = 0.44$). No significant change in MMP-2 activity was observed after LPS treatment or between the different genotypes (Figure 2B).

MMP-3 Activity Is Increased in COX-$2^{-/-}$ Mice but Decreased in COX-$1^{-/-}$ Mice 24 h After LPS

Stromelysin-1 (MMP-3) has been also shown to participate to LPS-induced BBB disruption (Gurney *et al*, 2006); therefore, we examined the effects of COX deletion on MMP-3 activity. In naïve mice, fluorescent enzymatic assay for MMP-3 activity was not different between COX-deficient and their respective wild-type mice (data not shown). LPS produced a significant increase (about three to four times) in MMP-3 activity after 24 h compared with vehicle-treated mice in both hippocampus and

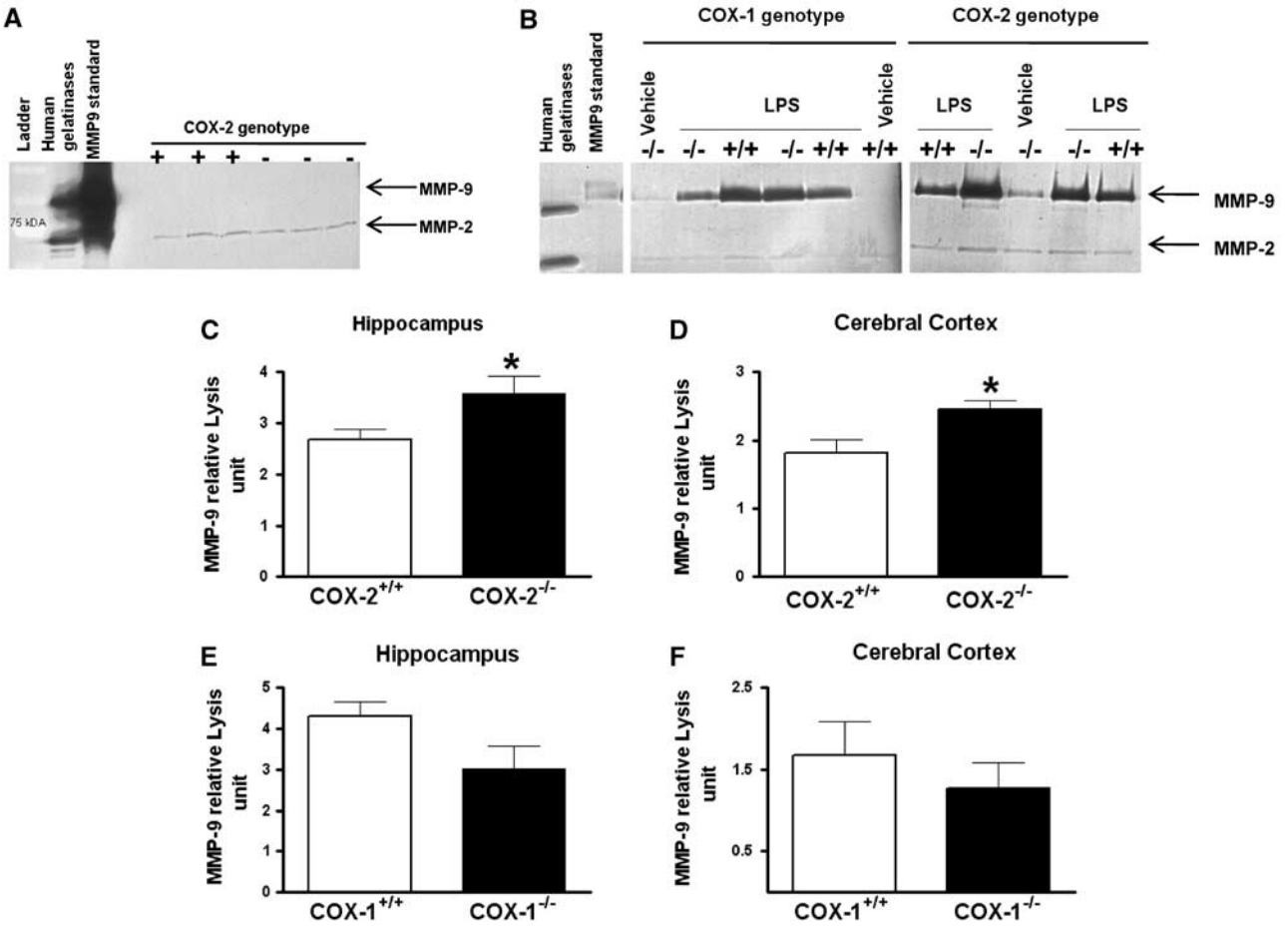

Figure 2 MMP-9 activity in hippocampus and cerebral cortex of COX-1 $^{+/+}$, COX-1$^{-/-}$, COX-2 $^{+/+}$, and COX-2$^{-/-}$ mice 24 h after LPS. (**A**) Representative gelatin zymogram showing the absence of MMP-9 activity in naïve COX-2-deficient and wild-type mice after 48 h incubation of the gels. Only a band around 72 kDa corresponding at MMP-2 was detected. (**B**) Representative gelatin zymogram showing the effects of COX-1 and COX-2 deletion on MMP-9 activity. Mice were injected intracerebroventricularly with 5 μg LPS. (**C**–**F**) Quantitative analysis of gelatinolytic activity of MMP-9 by zymography in hippocampus and cerebral cortex of LPS-injected COX-2 $^{+/+}$ ($n = 8$), COX-2$^{-/-}$ ($n = 5$), COX-1 $^{+/+}$ ($n = 5$), and COX-1$^{-/-}$ ($n = 6$) mice. Densitometric analysis of lytic zones at 72 kDa, corresponding to pro-MMP-2 activity, showed no significant change among treatments (data not shown). Data are presented as mean ± s.e.m. of the 98-kDa band in arbitrary densitometric units. *$P < 0.05$ versus LPS-injected respective wild type.

cerebral cortex (Figures 3A to 3D). MMP-3 activity was significantly increased in LPS-injected COX-2$^{-/-}$ mice compared with COX-2$^{+/+}$ mice in both hippocampus (Figure 3A; $P < 0.001$) and cerebral cortex (Figure 3B; $P < 0.01$). In contrast, MMP-3 activity was significantly decreased in LPS-injected COX-1$^{-/-}$ compared with COX-1$^{+/+}$ mice, in both brain areas (Figures 3C and 3D; $P < 0.001$), indicating that MMP-3 activity contributes to the differential effects of COX-1 and COX-2 deficiency on BBB disruption.

Gene Expression of Timp-1, Cxcl10, Cd45, and Icam-1 Is Differently Regulated in the Brain of COX-2$^{-/-}$ and COX-1$^{-/-}$ Mice After LPS

To assess the role of COX-2 deletion in worsening LPS-induced BBB disruption we examined the expression of several genes known to modulate BBB integrity, such as Timp-1, factor that mediates tissue penetration, the chemokine Cxcl10 implicated in the attraction of monocytes/macrophages, Icam-1, which is an important endothelial adhesion molecule for the immune cells, and Cd45 a pan-leukocyte marker. LPS significantly increased the expression of *Timp-1*, *Cxcl10*, *Cd45,* and *Icam-1* mRNA in all genotype (Figures 4A and 4B). However, the mRNA levels of these genes were higher in COX-2$^{-/-}$ compared with COX-2$^{+/+}$ mice after LPS (Figure 4A). On the contrary, the mRNA levels of *Timp-1*, *Cxcl10,* and *Cd45* were decreased in COX-1$^{-/-}$ compared with COX-1$^{+/+}$ mice after LPS (Figure 4B), except for *Icam-1* mRNA level.

Discussion

We have shown earlier that COX-1 and COX-2 have distinct roles during excitotoxic brain damage (Toscano *et al*, 2008*a*, *b*) and in LPS-induced acute

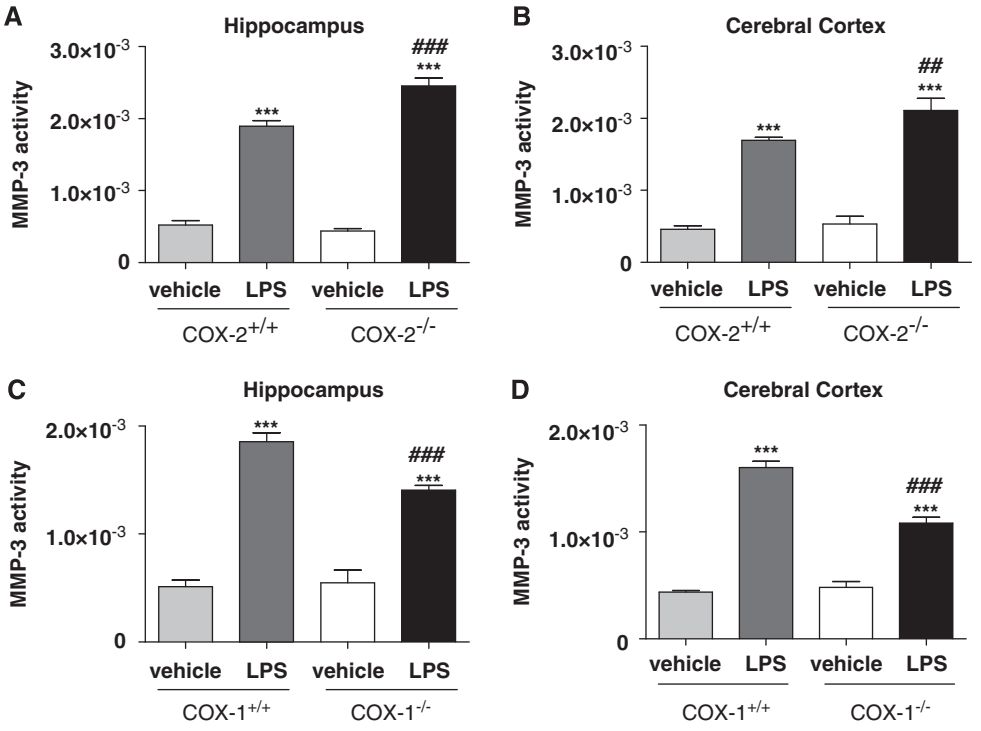

Figure 3 MMP-3 activity in hippocampus and cerebral cortex of COX-1 $^{+/+}$, COX-1$^{-/-}$, COX-2 $^{+/+}$, and COX-2$^{-/-}$ mice 24 h after LPS. Hippocampal and cortical MMP-3 activity were similar in vehicle-injected mice for both COX genotypes. LPS-induced increase in MMP-3 activity was higher in COX-2$^{-/-}$ mice (**A**, **B**) whereas it was reduced in COX-1$^{-/-}$ mice (**C**, **D**) as compared with their respective wild-type controls. Data are presented as mean velocity (relative fluorescence unit) ± s.e.m. (Vehicle-injected mice $n = 3$ to 4; LPS-injected mice, $n = 5$ to 8). $^{***}P < 0.001$ versus vehicle-injected mice; $^{\#\#}P < 0.01$, $^{\#\#\#}P < 0.001$ versus LPS-injected wild-type mice.

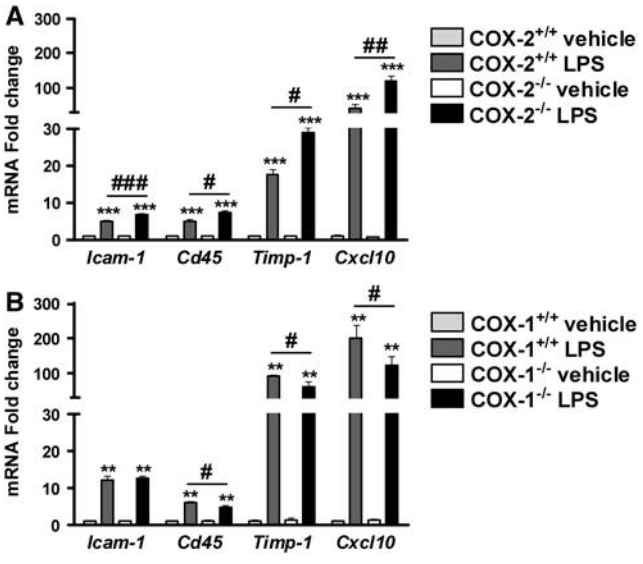

Figure 4 Effects of COX-2 and COX-1 deficiency on LPS-induced expression of mediators of BBB disruption and regulators of brain infiltration by immune cells. Quantitative real-time-PCR analysis of whole brain *Timp-1*, *Cxcl10*, *Cd45*, *Icam-1* for COX-2 $^{+/+}$, COX-2$^{-/-}$, COX-1 $^{+/+}$, and COX-1$^{-/-}$ mice 24 h after intracerebroventricular injection of LPS or vehicle. Data are presented as mean ± s.e.m. ($n = 4$ to 6). $^{**}P < 0.01$ $^{***}P < 0.001$ versus vehicle-injected mice; $^{\#}P < 0.05$, $^{\#\#}P < 0.01$, $^{\#\#\#}P < 0.001$ versus LPS-injected wild-type mice.

neuroinflammation (Aid *et al*, 2008; Choi *et al*, 2008). In this study, we used quantitative MRI combined with molecular techniques to investigate how COX-1 and COX-2 specifically modulate BBB integrity during LPS-induced innate immune activation. We showed that COX-2$^{-/-}$ mice exhibit an increase in LPS-induced BBB disruption in the whole brain and the hippocampus, mediated by an increase in MMP-9 and MMP-3 activities. We also showed that COX-1 deletion reduced the MMP-3 activity with no change in MMP-9 activity, although it did not significantly change the LPS-induced BBB permeability. These results further support the hypothesis that COX-1 and COX-2 mediate differential effects during the neuroinflammatory response, especially in maintaining the integrity of the neurovascular unit.

In physiological conditions, COX-1 and COX-2 have been shown to have distinct roles in cerebrovascular coupling. Specifically, COX-1 is important in the maintenance of resting cerebrovascular tone and in selected responses of the cerebral circulation, whereas COX-2 is involved in functional hyperemia (Niwa *et al*, 2000, 2001; Stefanovic *et al*, 2006). This study provides new evidence for the specific action and the functional significance of COX-1 and COX-2 during neuroinflammation. The experimental model of isolated central nervous system inflammation we used in this study has been shown to result in pathophysiological changes characteristic of bacter-

ial meningitis, including BBB breakdown, recruitment of neutrophils, and generation of meningeal inflammation (Mun-Bryce and Rosenberg, 1998).

The integrity of the BBB during neuroinflammation is highly dependent on the endothelial status, the elaboration of cytokines and chemokines, and the recruitment of circulating proinflammatory cells (Zlokovic, 2008). In this study, we showed that COX-2 deletion increases, whereas COX-1 deletion tends to reduce LPS-induced increase in BBB permeability and that MMP-3 activity contributes to this differential effect. Several studies agreed on the increased expression of COX-2 in endothelial cells after central or systemic injection of endotoxin or cytokines (Cao *et al*, 1998, 1999; Laflamme *et al*, 1999). Although LPS is a well-known primary activator of microglia in the central nervous system, COX-2 expression induced by LPS seems restricted to endothelial cells, with little evidence of expression in microglia or macrophage cells (Cao *et al*, 1999). There are conflicting data on the effect of COX inhibition on BBB permeability. *In vitro* studies showed that indomethacin, a COX-1 preferential inhibitor, and NS-398, a selective COX-2 inhibitor, both attenuated the cytokines-induced increase in transendothelial electrical resistance in endothelial cells (de Vries *et al*, 1996; Mark *et al*, 2001). Celecoxib, another COX-2 selective inhibitor, also has been shown to decrease the expression of tight junction proteins and of the vascular marker Icam *in vitro* (Germann *et al*, 2008). However, *in vivo* acute post administration of indomethacin, a preferential COX-1 inhibitor, but not nimesulide, a COX-2 selective inhibitor, attenuated TNF-α-induced BBB disruption (Candelario-Jalil *et al*, 2007*b*). Explanation for this disparity may lie in the lack of complete inhibition of one isoform over the other by the NSAID used. For instance, nimesulide is not a 'highly' selective COX-2 inhibitor, therefore depending on the dose and the dosing paradigm (acute versus chronic), either not a sufficient inhibition of COX-2 is reached or COX-1 is also inhibited. The time of treatment may also have an important function. For instance, COX-2 selective inhibition has been linked to either attenuation or potentiation of kainate-induced excitotoxic damage depending on whether the treatment was given before or after kainate (Candelario-Jalil *et al*, 2000; Kunz and Oliw, 2001; Toscano *et al*, 2008*b*). In agreement with our *in vivo* results, a recent study reported that chronic pretreatment with nimesulide precipitated the encephalopathy and exacerbated neuronal death in an experimental model of Wernicke's encephalopathy (Gu *et al*, 2008).

One possible explanation for the differential effects of COX-1 and COX-2 on BBB integrity may lie in MMP-3 (stromelysin-1) and MMP-9 (gelatinase B), which are two major inducible MMPs that have been recently identified during the neuroinflammatory response as causal mediators of BBB damage and infiltration of blood-borne cells (Candelario-Jalil *et al*, 2009). We showed that the activity of MMP-9 and MMP-3 is increased after LPS in the COX-$2^{-/-}$ mice, and that their increase paralleled the LPS-induced BBB damage. Our data further confirm the role of MMP-9 and MMP-3 activities in mediating BBB permeability and also link those activities to a COX-dependent pathway. MMPs can be produced by all cell types in the brain including microglia, astrocytes, neurons, and endothelial cells (Rosenberg, 2002). However, a recent *in vitro* study showed that MMPs are major inflammatory mediators released by activated microglia (Woo *et al*, 2008). As COX-$2^{-/-}$ mice display an exacerbated inflammatory response, with increases in microglia activation and in inflammatory mediators such as cytokines and chemokines (Aid *et al*, 2008), MMPs produced by activated microglia are likely to mediate the increased LPS-induced BBB disruption. MMPs are also released by white blood cells to facilitate the passage of leukocytes across the BBB: activated microglia, through the release of chemokines can also further increase the number/and or the activation state of leukocytes recruited into the inflamed brain, contributing to the exacerbated inflammatory response and BBB damage in the LPS-injected COX-$2^{-/-}$ mice (Figure 5).

Interestingly, COX-1 deletion significantly decreases MMP-3 activity in both hippocampus and cerebral cortex, whereas MMP-9 activity was not significantly changed in the LPS-injected COX-$1^{-/-}$ mice. Although the discrepancy between MMPs may be ascribed to the differential sensitivity of the methods used to measure MMP-9 activity (gelatin zymography) and MMP-3 activity (fluorometric assay), it is possible that MMP-3 is the key player in mediating the differential effects of COX-1 and COX-2 deficiency on LPS-induced BBB disruption (Figure 5). Indeed, the reduced MMP-3 activity observed in the COX-$1^{-/-}$ mice are in agreement with the decrease in the expression of proinflammatory cytokines, chemokines, and oxidative stress markers, and with the reduction of glial activation and neuronal damage in response to LPS previously reported in the COX-$1^{-/-}$ mice (Choi *et al*, 2008). Nevertheless, we could only detect a trend of a decrease in LPS-induced BBB breakdown in COX-$1^{-/-}$ compared with COX-$1^{+/+}$ mice ($P=0.06$), suggesting that the change in cytokines/chemokines expression, glial activation, MMP-3 and MMP-9 activities are likely the causative events to the change in BBB permeability in response to LPS.

Cytokines such as IL-1β and TNF-α have been shown to mediate BBB disruption *in vivo* (Blamire *et al*, 2000; Sibson *et al*, 2002). We previously showed that brain levels of IL-1β, TNF-α, and MIP-1α are downregulated in COX-$1^{-/-}$ and upregulated in COX-$2^{-/-}$ mice compared with their respective wild type, after intracerebroventricular LPS (Aid *et al*, 2008; Choi *et al*, 2008). In this study, we also show that the leukocyte attracting chemokine *Cxcl10*, the pan-leukocyte marker *Cd45*, and the adhesion

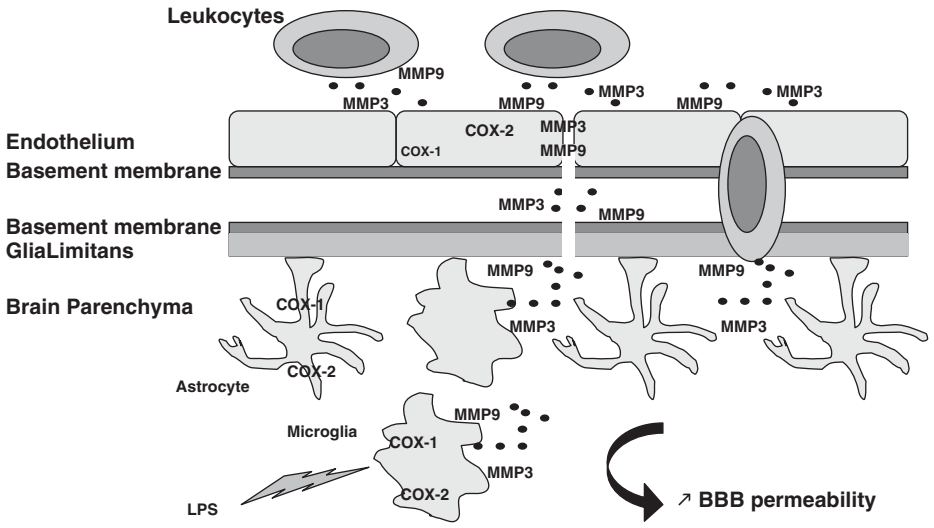

Figure 5 Distinct effects of COX-1 and -2 deletion on LPS-induced BBB disruption. Lipopolysaccharide (LPS) activates primarily microglia, which releases cytokines, chemokines, MMP-9, and MMP-3. The neuroinflammatory response, through chemokines and cytokines, also propagates to the surrounding cells such as astrocytes and endothelial cells. Chemokines initiate signals that lead to leukocyte arrest, adhesion, and extravasation through the endothelium and perivascular space. The action of MMP-9 and MMP-3, released by activated microglia and leukocytes, allow leukocyte entry into the brain parenchyma by attacking the basement membrane and glia limitans. Although present in all cell types, COX-1 is mainly found in microglia, and COX-2 is predominant in neurons and endothelial cells. COX-1 deletion decreases chemokine expression and MMP-3 activity, which most likely will attenuate LPS-induced increase in BBB permeability. However, COX-2 deletion exacerbates LPS-induced BBB disruption, through an increase in chemokine release and MMP-9 and MMP-3 activities.

molecule *Icam-1* are upregulated in the COX-$2^{-/-}$ compared with COX-$2^{+/+}$ mice after intracerebroventricular LPS. On the contrary, the gene expression of *Cxcl10* and *Cd45* are downregulated in the COX-$1^{-/-}$ compared with COX-$1^{+/+}$ mice after intracerebroventricular LPS. IL-1β and TNF-α are particularly important for activation of the endothelium and leukocytes; chemokines control leukocytes extravasation and chemotaxis toward the affected tissues and the endothelial adhesion molecule Icam-1 is essential to leukocytes adhesion and transmigration into the inflamed neural tissue (Man *et al*, 2007). As the expression of the above markers paralleled the LPS-induced BBB damage, they are likely to further contribute to the differential effect of COX-1 and COX-2 deficiency on the neuroinflammatory response by promoting leukocytes infiltration into the inflamed brain.

Conclusion

These findings prove in knockout models that COX-1 and COX-2 display unique roles in mediating BBB disruption during activation of the innate immune response. In particular, in this model COX-2 deletion increased the LPS-induced BBB disruption, through an increase in MMP-9 and MMP-3 activities, and in gene expression of chemokine (*Cxcl10*), leukocyte (*Cd45*), and endothelial (*Icam-1*) markers; whereas COX-1 deletion decreased MMP-3 activity and gene expression of *Cxcl10* and *Cd45*. This study provides new evidence for the specific action and the functional significance of COX-1 and COX-2 during neuroinflammation. As alteration of BBB integrity or function seems to be a common event in neuropathologies with a marked inflammatory component, such as Parkinson's disease, Alzheimer's disease, multiple sclerosis, and bacterial meningitis (Weiss *et al*, 2009; Zlokovic, 2008), our data suggest that the use of COX-1 preferential inhibitors should be preferred to the use of specific COX-2 inhibitors to preserve BBB integrity. This study also warrants new research into the mechanisms underlying the specific roles of COX-1 and COX-2 in the cross-talk between the blood–central nervous system barrier and the innate immune system.

Acknowledgements

We thank Dr Robert Langenbach for providing COX-$1^{-/-}$, COX-$2^{-/-}$, and wild-type mice. We thank Xian Feng (Lisa) Zhang for her technical help in preparing the mice for MRI. We also thank Dr Christopher D Toscano for useful experimental suggestions and discussion and Dr Alan B Zonderman for statistical help. This work was supported by the NIH Intramural Research Program (NIA and NINDS) and by grants from the American Heart Association (0720160Z to ECJ) and the NIH (5R01NS04547 to GAR).

Conflict of interest

The authors declare no conflict of interest.

References

Aid S, Bosetti F (2007) Gene expression of cyclooxygenase-1 and Ca(2+)-independent phospholipase A(2) is altered in rat hippocampus during normalaging. *Brain Res Bull* 73:108–13

Aid S, Langenbach R, Bosetti F (2008) Neuroinflammatory response to lipopolysaccharide is exacerbated in mice genetically deficient in cyclooxygenase-2. *J Neuroinflammation* 5:17

Blamire AM, Anthony DC, Rajagopalan B, Sibson NR, Perry VH, Styles P (2000) Interleukin-1beta -induced changes in blood-brain barrier permeability, apparent diffusion coefficient, and cerebral blood volume in the rat brain: a magnetic resonance study. *J Neurosci* 20:8153–9

Candelario-Jalil E, Ajamieh HH, Sam S, Martinez G, Leon Fernandez OS (2000) Nimesulide limits kainate-induced oxidative damage in the rat hippocampus. *Eur J Pharmacol* 390:295–8

Candelario-Jalil E, Gonzalez-Falcon A, Garcia-Cabrera M, Leon OS, Fiebich BL (2007*a*) -ischaemic treatment with the cyclooxygenase-2 inhibitor nimesulide reduces blood-brain barrier disruption and leukocyte infiltration following transient focal cerebral ischaemia in rats. *J Neurochem* 100:1108–20

Candelario-Jalil E, Taheri S, Yang Y, Sood R, Grossetete M, Estrada EY, Fiebich BL, Rosenberg GA (2007*b*) Cyclooxygenase inhibition limits blood-brain barrier disruption following intracerebral injection of tumor necrosis factor-alpha in the rat. *J Pharmacol Exp Ther* 323: 488–98

Candelario-Jalil E, Yang Y, Rosenberg GA (2009) Diverse roles of matrix metalloproteinases and tissue inhibitors of metalloproteinases in neuroinflammation and cerebral ischemia. *Neuroscience* 158:983–94

Cao C, Matsumura K, Ozaki M, Watanabe Y (1999) Lipopolysaccharide injected into the cerebral ventricle evokes fever through induction of cyclooxygenase-2 in brain endothelial cells. *J Neurosci* 19:716–25

Cao C, Matsumura K, Yamagata K, Watanabe Y (1998) Cyclooxygenase-2 is induced in brain blood vessels during fever evoked by peripheral or central administration of tumor necrosis factor. *Brain Res Mol Brain Res* 56:45–56

Choi SH, Langenbach R, Bosetti F (2008) Genetic deletion or pharmacological inhibition of cyclooxygenase-1 attenuate lipopolysaccharide-induced inflammatory response and brain injury. *FASEB J* 22:1491–501

de Vries HE, Blom-Roosemalen MC, de Boer AG, van Berkel TJ, Breimer DD, Kuiper J (1996) Effect of endotoxin on permeability of bovine cerebral endothelial cell layers *in vitro*. *J Pharmacol Exp Ther* 277: 1418–1423

Fridman R, Toth M, Chvyrkova I, Meroueh SO, Mobashery S (2003) Cell surface association of matrix metalloproteinase-9 (gelatinase B). *Cancer Metastasis Rev* 22: 153–66

Germann B, Neuhaus W, Hofer-Warbinek R, Noe CR (2008) Applying blood-brain barrier *in vitro* models to study the influence of drugs on endothelial cells—effects of selected COX-inhibitors. *Pharmazie* 63:303–7

Goralski KB, Abdulla D, Sinal CJ, Arsenault A, Renton KW (2005) Toll-like receptor-4 regulation of hepatic Cyp3a11 metabolism in a mouse model of LPS-induced CNS inflammation. *Am J Physiol Gastrointest Liver Physiol* 289:G434–43

Gruetter R (1993) Automatic, localized *in vivo* adjustment of all first- and second-order shim coils. *Magn Reson Med* 29:804–11

Gu B, Desjardins P, Butterworth RF (2008) Selective increase of neuronal cyclooxygenase-2 (COX-2) expression in vulnerable brain regions of rats with experimental Wernicke's encephalopathy: effect of nimesulide. *Metab Brain Dis* 23:175–87

Gurney KJ, Estrada EY, Rosenberg GA (2006) Blood-brain barrier disruption by stromelysin-1 facilitates neutrophil infiltration in neuroinflammation. *Neurobiol Dis* 23:87–96

Keene CD, Chang R, Stephen C, Nivison M, Nutt SE, Look A, Breyer RM, Horner PJ, Hevner R, Montine TJ (2009) Protection of hippocampal neurogenesis from toll-like receptor 4-dependent innate immune activation by ablation of prostaglandin E2 receptor subtype EP1 or EP2. *Am J Pathol* 174:2300–9

Kunz T, Oliw EH (2001) Nimesulide aggravates kainic acid-induced seizures in the rat. *Pharmacol Toxicol* 88:271–6

Laflamme N, Lacroix S, Rivest S (1999) An essential role of interleukin-1beta in mediating NF-kappaB activity and COX-2 transcription in cells of the blood-brain barrier in response to a systemic and localized inflammation but not during endotoxemia. *J Neurosci* 19:10923–30

Livak KJ, Schmittgen TD (2001) Analysis of relative gene expression data using real-time quantitative PCR and the 2(−Delta Delta C(T)) method. *Methods* 25:402–8

Man S, Ubogu EE, Ransohoff RM (2007) Inflammatory cell migration into the central nervous system: a few new twists on an old tale. *Brain Pathol* 17:243–50

Mark KS, Trickler WJ, Miller DW (2001) Tumor necrosis factor-alpha induces cyclooxygenase-2 expression and prostaglandin release in brain microvessel endothelial cells. *J Pharmacol Exp Ther* 297:1051–8

Mikulis DJ, Roberts TP (2007) Neuro MR: protocols. *J Magn Reson Imaging* 26:838–47

Milatovic D, Zaja-Milatovic S, Montine KS, Shie FS, Montine TJ (2004) Neuronal oxidative damage and dendritic degeneration followingactivation of CD14-dependent innate immune response *in vivo*. *J Neuroinflammation* 1:20

Mun-Bryce S, Rosenberg GA (1998) Gelatinase B modulates selective opening of the blood-brain barrier during inflammation. *Am J Physiol* 274:R1203–11

Nagase H, Fields CG, Fields GB (1994) Design and characterization of a fluorogenic substrate selectively hydrolyzed by stromelysin 1 (matrix metalloproteinase-3). *J Biol Chem* 269:20952–7

Niwa K, Araki E, Morham SG, Ross ME, Iadecola C (2000) Cyclooxygenase-2 contributes to functional hyperemia in whisker-barrel cortex. *J Neurosci* 20:763–70

Niwa K, Haensel C, Ross ME, Iadecola C (2001) Cyclooxygenase-1 participates in selected vasodilator responses of the cerebral circulation. *Circ Res* 88:600–8

Patlak CS, Blasberg RG, Fenstermacher JD (1983) Graphical evaluation of blood-to-brain transfer constants from multiple-time uptake data. *J Cereb Blood Flow Metab* 3:1–7

Paxinos G, Franklin KBJ (eds) (2001) *The mouse brain in stereotaxic coordinates*. San Diego, CA: Academic Press

Rosenberg GA (2002) Matrix metalloproteinases in neuroinflammation. *Glia* 39:279–91

Sibson NR, Blamire AM, Perry VH, Gauldie J, Styles P, Anthony DC (2002) TNF-alpha reduces cerebral blood volume and disrupts tissue homeostasis via an endothelin- and TNFR2-dependent pathway. *Brain* 125:2446–59

Stefanovic B, Bosetti F, Silva AC (2006) Modulatory role of cyclooxygenase-2 in cerebrovascular coupling. *Neuroimage* 32:23–32

Takanashi Y, Shinonaga M, Naitoh M, Noguchi N (2000) Magnetic resonance imaging with gadolinium DTPA enhancement in patients with acute head injury. *J Neurotrauma* 17:359–65

Toscano CD, Kingsley PJ, Marnett LJ, Bosetti F (2008*a*) NMDA-induced seizure intensity is enhanced in COX-2 deficient mice. *Neurotoxicology* 29:1114–20

Toscano CD, Prabhu VV, Langenbach R, Becker KG, Bosetti F (2007) Differential gene expression patterns in cyclooxygenase-1 and cyclooxygenase-2 deficient mouse brain. *Genome Biol* 8:R14

Toscano CD, Ueda Y, Tomita YA, Vicini S, Bosetti F (2008*b*) Altered GABAergic neurotransmission is associated with increased kainate-induced seizure in prostaglandin-endoperoxide synthase-2 deficient mice. *Brain Res Bull* 75:598–609

Weiss N, Miller F, Cazaubon S, Couraud PO (2009) The blood-brain barrier in brain homeostasis and neurological diseases. *Biochim Biophys Acta* 1788:842–57

Woo MS, Park JS, Choi IY, Kim WK, Kim HS (2008) Inhibition of MMP-3 or -9 suppresses lipopolysaccharide-induced expression of proinflammatory cytokines and iNOS in microglia. *J Neurochem* 106: 770–80

Zlokovic BV (2008) The blood-brain barrier in health and chronicneurodegenerative disorders. *Neuron* 57: 178–201